Aseev, N., Shprits, Y., Drozdov, A. Y., Kellerman, A. C. (2016): Numerical applications of the advective-diffusive codes for the inner magnetosphere. - *Space Weather*, *14*, 11, pp. 993—1010.

DOI: http://doi.org/10.1002/2016SW001484

AGU PUBLICATIONS

Space Weather

RESEARCH ARTICLE
10.1002/2016SW001484

Numerical applications of the advective-diffusive codes for the inner magnetosphere

N. A. Aseev[1,2], Y. Y. Shprits[1,2,3], A. Y. Drozdov[3], and A. C. Kellerman[3]

[1]Section 2.3 Earth's Magnetic Field, GFZ German Research Centre for Geosciences, Potsdam, Germany, [2]Institute of Physics and Astronomy, University of Potsdam, Potsdam, Germany, [3]Earth, Planetary, and Space Sciences, University of California, Los Angeles, California, USA

Key Points:
- A set of convenient analytical solutions for testing codes for the inner magnetosphereis presented
- The basic features of the numerical schemes of the VERB-4D code are demonstrated
- The order of numerical schemes has significant influence on magnetospheric convection modeling

Correspondence to:
N. A. Aseev,
nikita.aseev@gfz-potsdam.de

Citation:
Aseev, N. A., Y. Y. Shprits, A. Y. Drozdov, and A. C. Kellerman (2016), Numerical applications of the advective-diffusive codes for the inner magnetosphere, *Space Weather*, *14*, 993–1010, doi:10.1002/2016SW001484.

Received 1 AUG 2016
Accepted 22 OCT 2016
Accepted article online 31 OCT 2016
Published online 8 NOV 2016

Abstract In this study we present analytical solutions for convection and diffusion equations. We gather here the analytical solutions for the one-dimensional convection equation, the two-dimensional convection problem, and the one- and two-dimensional diffusion equations. Using obtained analytical solutions, we test the four-dimensional Versatile Electron Radiation Belt code (the VERB-4D code), which solves the modified Fokker-Planck equation with additional convection terms. The ninth-order upwind numerical scheme for the one-dimensional convection equation shows much more accurate results than the results obtained with the third-order scheme. The universal limiter eliminates unphysical oscillations generated by high-order linear upwind schemes. Decrease in the space step leads to convergence of a numerical solution of the two-dimensional diffusion equation with mixed terms to the analytical solution. We compare the results of the third- and ninth-order schemes applied to magnetospheric convection modeling. The results show significant differences in electron fluxes near geostationary orbit when different numerical schemes are used.

1. Introduction

The last decades gave rise to swift development of codes modeling the near-Earth space environment. Ring current and radiation belt codes have particular importance, since the codes provide predictive capabilities for the extremely variable environment, where many satellites operate and may be damaged by charged particles penetrating satellite shielding.

Numerical details of existing ring current and radiation belt codes are rarely discussed in the literature, yet they play a very important role for the accuracy of the simulations and computational time requirements. Most of the codes are validated by comparison with data, while the basic validation of the accuracy of numerical methods has not been done or discussed in the literature. Inaccurate or unstable numerical methods may lead to significant errors, complicate the direct validation of the codes with data, or render the comparison with data meaningless. Accurate and stable numerical methods allow us to rely on results of the codes and even explain new physical phenomena.

The goal of this work is to present a convenient set of analytical solutions for testing advective-diffusive codes for the inner magnetosphere and to demonstrate the fundamental features of the numerical schemes implemented in the four-dimensional Versatile Electron Radiation Belt code (the VERB-4D code [*Shprits et al.*, 2015]). The VERB-4D code is an advective-diffusive code modeling the dynamics of the Earth's electron radiation belts. Presented in this study are numerical methods and test results of these methods, which can be extended to any advective-diffusive code for the Earth's inner magnetosphere.

The Earth's radiation belts consist of electrons and ions (mostly protons) trapped by the Earth's magnetic field. The energetic and relativistic electrons (from ≈100 to 900 keV) usually form a two-zone structure, while above 900 keV electrons are only presented in the outer zone [*Fennell et al.*, 2015]. The inner zone is located at radial distances between 1 and 2 Earth radii and is very stable [*Williams and Smith*, 1965; *Pfitzer and Winckler*, 1968]. The outer zone can be extremely variable, and the electron dynamics in the outer zone depends significantly on geomagnetic conditions [*Rothwell and McIlwain*, 1960; *Craven*, 1966]. Electron flux between the inner and outer zones is usually several orders of magnitude lower than the flux in the belt zone but can be refilled or may even form a new belt [*Baker et al.*, 2004; *Shprits et al.*, 2011]. This gap between the belts is referred to as a slot region [*Russell and Thorne*, 1970; *Vernov et al.*, 1969].

Relativistic electrons in the radiation belts undergo three different types of periodic motion: gyration around geomagnetic field lines, bouncing between the mirror points, and azimuthal drift around the Earth. Adiabatic invariants μ, J, and Φ are attributed to these types of motion, respectively [*Kellogg*, 1959; *Roederer*, 1970; *Schulz and Lanzerotti*, 1974; *Walt*, 1994]. The invariants stay approximately constant when changes in the magnetic field happen slowly in comparison with the time scale of corresponding periodic motion. Thus, once being trapped, the particle will remain trapped forever under slow variations of environmental parameters. However, resonant interactions with plasma waves can violate the invariants, if the characteristic disturbance time is comparable with the time scale of the corresponding type of periodic motion. Since the number of particles in the radiation belts is large, we can often describe particle behavior collectively in terms of phase space density (PSD). Assuming that waves in the belts are incoherent at various radial distances and magnetic local times (MLT) and that amplitudes of waves are much smaller than the background field, wave-particle interactions can be approximated as a diffusion process [*Kennel and Engelmann*, 1966; *Lerche*, 1968].

Diffusion processes in the radiation belts can be divided into radial and local diffusion. Radial diffusion [*Kellogg*, 1959; *Falthammar*, 1965; *Schulz and Eviatar*, 1969] describes the violation of the invariant Φ by resonant interactions with ULF waves [*Lanzerotti and Morgan*, 1973; *Brautigam and Albert*, 2000]. It leads to inward or outward radial motion of charged particles, depending on the sign of PSD gradient. Inward radial diffusion is a dominant mechanism of electron energization [*Hudson et al.*, 2001; *Elkington et al.*, 2003] due to betatron and Fermi acceleration, and outward radial diffusion can lead to losses driven by magnetopause shadowing [*Shprits et al.*, 2006a, 2008a]. Such processes can be accompanied by two-dimensional local diffusion [*Kennel and Engelmann*, 1966; *Lerche*, 1968], which is responsible for the violation of μ and J. Pitch angle diffusion scatters electrons into the loss cone and forces them to precipitate into the Earth's atmosphere. In turn, energy diffusion produces acceleration of electrons. Interactions with plasmaspheric hiss waves, lightning-generated whistlers, and anthropogenic VLF waves are responsible for the pitch angle scattering inside the plasmasphere and produces only negligible energy diffusion. Acting outside the plasmasphere, chorus waves are responsible for the pitch angle scattering as well. Electron acceleration mostly happens locally on the night side due to the interactions with chorus waves. Interactions of high-energy electrons with electromagnetic ion cyclotron waves can also produce electron losses [*Thorne and Kennel*, 1971; *Usanova et al.*, 2014; *Thorne and Kennel*, 1971; *Kersten et al.*, 2014; *Usanova et al.*, 2014]. They are most efficient at multi-MeV energies [*Shprits et al.*, 2013; *Drozdov et al.*, 2015]. Radial diffusion and local diffusion are reviewed in details in *Shprits et al.* [2008a, 2008b].

Another important process is magnetospheric convection [*Dungey*, 1961; *Axford*, 1969]. The solar wind generates an electric field directing from dawn to dusk inside the magnetosphere [*Schulz and Lanzerotti*, 1974] and transports electrons from the plasma sheet inward by the $\mathbf{E} \times \mathbf{B}$ drift. Storm time injections of low-energy plasma sheet electrons provide seed population and are crucial for the dynamics of ring current and radiation belts during disturbed geomagnetic conditions. For MeV electrons, advection due to gradient-curvature drift dominates over $\mathbf{E} \times \mathbf{B}$ transport.

The modified three-dimensional Fokker-Planck equation comprises both radial and local diffusion and describes the evolution of PSD. Originally, it is written in the (μ, J, and Φ) coordinate system, but more convenient systems can be applied to the equation, using the corresponding transformation of coordinates and diffusion coefficients [*Haerendel*, 1968; *Schulz and Lanzerotti*, 1974]. The Fokker-Planck equation can be supplemented by additional advection (often referred to as "convection") terms to take into account radial and azimuthal convection [*Shprits et al.*, 2015].

The first code modeling the dynamics of the electron radiation belts was the Salammbô code [*Beutier and Boscher*, 1995]. The original version of the code solved the three-dimensional Fokker-Planck equation in terms of adiabatic invariants. The Salammbô code incorporates radial diffusion, cosmic ray albedo neutron decay, pitch angle scattering by plasmaspheric hiss, and Coulomb collisions. Unfortunately, details on numerical implementation and boundary conditions of the first versions of the code were not provided in publications. The VERB code [*Shprits et al.*, 2008a, 2009; *Subbotin and Shprits*, 2009; *Subbotin et al.*, 2010, 2011a, 2011b] has been developed to solve the three-dimensional Fokker-Planck equation and takes into account radial, pitch angle, energy, and mixed diffusion, and additional electron sources or losses. The code utilizes the two-grid approach [*Subbotin and Shprits*, 2009]. According to this approach, two different grids are used for the solution of radial and local diffusion equations. A variety of codes was developed on the basis of similar approaches (e.g., the DREAM3D code [*Tu et al.*, 2013], the STEERB code [*Zhang et al.*, 2014], and the BAS code [*Glauert et al.*, 2014]). Though the two-grid approach is convenient for the formulation of boundary conditions, the approach

may lead to an increase in computational time, possible computational instabilities, and numerical errors due to inaccuracies of the interpolation. To avoid the interpolation, a new set of variables was introduced [*Subbotin and Shprits*, 2012], and the one-grid approach was implemented in the VERB-4D code.

A number of ring current codes have been developed for the convection of electrons and ions. The RAM code [*Jordanova et al.*, 1996, 1997] and the HEIDI model [*Liemohn et al.*, 2001; *Ilie et al.*, 2012] solve the bounce-averaged kinetic equation. The equation describes the evolution of PSD as an advective process in coordinates consisting of radial distance, geomagnetic east longitude, kinetic energy, and cosine of the equatorial pitch angle. Such loss mechanisms as charge exchange, Coulomb collisions, wave-particle interactions, and absorption in the atmosphere are also taken into account. The RBE model [*Fok et al.*, 2008] is a kinetic model that calculates the temporal variation of PSD of energetic electrons. The RBE model includes drifts of the particle population along magnetic field lines and in MLT, local diffusion due to wave-particle interactions, and losses to the loss cone. The IMPTAM code [*Ganushkina et al.*, 2006, 2012] is an advective code, which follows the distributions of ions and electrons. Charge exchange with neutral hydrogen in the upper atmosphere, Coulomb collisions, and convective outflow through the magnetopause are included into the IMPTAM.

A more comprehensive inner and middle magnetospheric model, the RCM code [*Toffoletto et al.*, 2003], uses a many fluid formalism to describe adiabatically drifting isotropic particle distributions in a self-consistently computed electric field and specified magnetic field. The successor of the RCM, the RCM-E code [*Lemon et al.*, 2004], is a combination of the RCM and magnetofriction equilibrium solver [*Hesse and Birn*, 1993]. The incorporated equilibrium solver provides a magnetic field model, which is consistent with RCM-computed pressures.

Complications of the mathematical description of the radiation belt dynamics results in application of numerical methods and techniques to the solution of high-dimensional problems. The difference in the associated time scales allows us to neglect mixed diffusion terms corresponding to the third invariant and split the solution of the three-dimensional Fokker-Planck equation into independent solutions of the one-dimensional radial diffusion and the two-dimensional local diffusion equations. Convection terms can be added to the splitted three-dimensional Fokker-Planck equation as extra fractional steps. The separation into physical processes makes it possible to implement the numerical schemes, describing independently each of the processes. Therefore, the most efficient and accurate schemes can be chosen for each physical process characterizing ring current and radiation belt dynamics.

Inner magnetospheric codes usually approximate convection terms in smooth regions using the Lax-Wendroff scheme, which is second-order accurate in space and time (e.g., RAM code [*Jordanova et al.*, 1996], HEIDI model [*Liemohn et al.*, 2004], and RBE model [*Fok et al.*, 1993]). (The order of a numerical scheme is the rate of convergence of the numerical solution to the exact solution, when the discretization step decreases) [*Godunov and Ryabenkii*, 1987]. The codes switch to the first-order scheme in the presence of strong gradients, where this scheme behaves better. For diffusion simulations, the most common are first- or second-order accurate in time and second-order accurate in space numerical schemes (e.g., DREAM3D, STEERB, BAS, and VERB codes).

In this work we present convenient analytical solutions for testing codes, which model the ring current-radiation belt system in the inner magnetosphere. The solutions are presented for the one-dimensional convection equation describing either radial or azimuthal convection, the two-dimensional convection equation taking into account both radial and azimuthal convection, the one-dimensional diffusion equation simulating radial diffusion, and the two-dimensional diffusion equation modeling local diffusion with mixed pitch angle and energy terms. We present results of testing implemented in the VERB-4D code numerical schemes on the basis of the provided analytical solutions. We study here how accuracy of numerical schemes affects results of simulations. Comparison of the third- and ninth-order schemes applied to idealized quiet time magnetospheric convection simulations is also presented.

The structure of the paper is organized as follows. In section 2 we briefly describe the mathematical formulation of the modified Fokker-Planck equation and the numerical algorithms, which constitute the core of the VERB-4D code. Section 3 is devoted to the convenient analytical solutions for testing codes and results of some tests made with the VERB-4D code. The influence of the order of numerical schemes on magnetospheric convection modeling is discussed section 4. The main conclusions are presented in section 5. Appendix A describes the Courant-Friedrichs-Lewy condition, and Appendix B contains details on the

universal limiter which eliminates unphysical oscillations of the high-order linear numerical schemes for the convection equation.

2. The Approach of the VERB-4D Code

The VERB-4D code has evolved from the one-dimensional [*Shprits et al.*, 2005], two-dimensional [*Shprits et al.*, 2006b], and three-dimensional [*Shprits et al.*, 2008a, 2009; *Subbotin and Shprits*, 2009; *Subbotin et al.*, 2010; *Kim et al.*, 2011; *Subbotin et al.*, 2011a, 2011b] versions of the VERB code. The VERB-4D code solves the modified Fokker-Planck equation with additional convection terms following the approach of *Subbotin and Shprits* [2012] and *Shprits et al.* [2015]:

$$\frac{\partial f}{\partial t} = -\langle v_\varphi \rangle \frac{\partial f}{\partial \varphi} - \langle v_R \rangle \frac{\partial f}{\partial R} + \frac{1}{G}\frac{\partial}{\partial L^*} G \langle D_{L^*L^*} \rangle \frac{\partial f}{\partial L^*} + \frac{1}{G}\frac{\partial}{\partial V} G \left[\langle D_{VV} \rangle \frac{\partial f}{\partial V} + \langle D_{VK} \rangle \frac{\partial f}{\partial K} \right] + \frac{1}{G}\frac{\partial}{\partial K} G \left[\langle D_{KV} \rangle \frac{\partial f}{\partial V} + \langle D_{KK} \rangle \frac{\partial f}{\partial K} \right] - \frac{f}{\tau}, \quad (1)$$

where L^*, K, and V are adiabatic invariants, $L^* = 2\pi B_0 R_E^2/\Phi$, R_E is the Earth's radii, B_0 is the magnetic field at the geomagnetic equator at the Earth's surface, $K = J/\sqrt{8m_0\mu}$, m_0 is particle rest mass, $V = \mu \cdot (K + 0.5)^2$, $f(\phi, R, V, K)$ is the phase space density, t represents time, φ is MLT, R is the radial distance from the center of the Earth, τ is electron lifetime related to scattering into the loss cone and magnetopause shadowing, $\langle v_\varphi \rangle$ and $\langle v_R \rangle$ are bounce-averaged drift velocities, $\langle D_{L^*L^*} \rangle$, $\langle D_{VV} \rangle$, $\langle D_{VK} \rangle$, $\langle D_{KV} \rangle$ and $\langle D_{KK} \rangle$ are bounce-averaged diffusion coefficients, and $G = -2\pi B_0 R_E^2 \sqrt{8m_0 V}/(K + 0.5)^3/L^{*2}$ is the Jacobian of coordinate transformation from (μ, J, Φ) to (V, K, L^*).

The VERB-4D code uses the operator splitting technique [*Marchuk*, 1990; *Press et al.*, 1992; *Subbotin and Shprits*, 2009], separating one-dimensional convection in MLT (first term of the right-hand side), one-dimensional convection in R (second term), one-dimensional radial diffusion (third term), and two-dimensional local diffusion (fourth and fifth terms). A loss term (last term) is divided between processes in accordance with the nature of losses (e.g., losses to the magnetopause are added after the convection step of calculations; losses to the loss cone are added to local diffusion).

The VERB-4D code solves equation (1) for PSD using only one grid in (ϕ, R, V, K) coordinate system. While this system is convenient for modeling convection and local diffusion processes, radial diffusion must be simulated in (ϕ, L^*, V, K) coordinates. To model radial diffusion, the VERB-4D code receives values of L^* as an input. The values of L^* are computed on the same (ϕ, R, V, K) grid, using realistic magnetic field model, and updated each time when configuration of the magnetic field changes. Adiabatic changes due to compression and expansion of the magnetic field are implicitly taken into account, using one-dimensional cubic spline interpolation of PSD [*Press et al.*, 1992] from previous to current values of L^* for all (ϕ, V, K) values, if L^* changes.

Time and space discretization methods can be applied for low-dimensional subproblems arising from the application of the operator splitting technique. We now describe them in more detail. The VERB-4D code solves one-dimensional convection equation using the ninth-order upwind scheme. (Upwind schemes take into account the direction of the convective flow by calculating spatial derivative upstream) [*Godunov and Ryabenkii*, 1987]. *Godunov* [1959] showed that high-order (higher than second order) linear numerical schemes for the one-dimensional convection equation suffer from artificial numerical oscillations leading to unphysical results. To eliminate the unphysical oscillations, the universal limiter is applied to high-order numerical schemes in the VERB-4D code (see Appendix B, *Leonard* [1991] and *Leonard and Niknafs* [1991] for more details). The universal limiter detects regions of unphysical oscillations and decreases the accuracy of the scheme to the first order. The universal limiter can produce slight amplitude error near points of local extrema of the transported profile, where changes in monotonicity are mistakenly recognized as short wavelength unphysical oscillations. The discriminator developed by *Leonard and Niknafs* [1991] is also implemented in the VERB-4D code to diminish this amplitude error. Time discretization of the one-dimensional convection equation is explicit (the value of the function at each spatial grid point can be explicitly calculated from the previous time step), which makes implemented schemes conditionally stable. The conditional stability requires the Courant-Friedrichs-Lewy condition to be satisfied, imposing the restrictions on the ratio of time step to space step (see Appendix A).

The one-dimensional diffusion equation is solved implicitly (numerical solution at the current time step is calculated involving information of the modeled system at both current and previous time steps) [*Godunov and Ryabenkii*, 1987]. The implicit scheme is unconditionally stable for any time step and has first-order accuracy in time and second-order accuracy in space. Such time and space discretization schemes require the inversion of tridiagonal matrix at each time step. The tridiagonal matrix algorithm [*Press et al.*, 1992] is used in the VERB-4D code to solve corresponding system of linear equations. The algorithm has linear complexity in the number of spatial nodes, which makes this algorithm computationally efficient. The discretization of the two-dimensional diffusion equation, including mixed diffusion terms, is also fully implicit, unconditionally stable, and has first-order accuracy in time and second-order accuracy in space. A direct solver implemented in LAPACK [*Anderson et al.*, 1999] is used for a system of linear equations resulting from the space discretization of the second order.

The computational grid of the VERB-4D code is uniform in ϕ, R coordinates, logarithmic in V coordinates, and either uniform or logarithmic in K coordinates. Since implemented schemes for convection equation are conditionally stable, the input time step is decreased automatically (if necessary) at the convection fractional steps to satisfy the Courant-Friedrichs-Lewy condition. The input time step is not changed at the diffusion fractional steps due to unconditional stability of corresponding schemes. This selective decrease in the time step reduces total computational time.

3. Theoretical Framework for Testing the Inner Magnetospheric Models

To demonstrate stability, accuracy, and advantages of techniques of the VERB-4D code, we separate corresponding blocks in the code in order to investigate only the behavior of chosen numerical schemes. We use artificial analytical profiles as initial and boundary conditions in accordance with the physical nature of simulated processes. We should note that all tests show properties of schemes in simple cases, since artificial profiles are obtained on the basis of strong assumptions (e.g., constant velocities or diffusion coefficients). Despite the induced simplicity, the analytical solutions are useful for understanding the behavior of schemes for smooth initial profiles and profiles with discontinuities or high gradients. Some results of testing the numerical schemes implemented in the VERB-4D code along with utilized analytical solutions are presented in this section.

3.1. One-Dimensional Convection

In the simplest form, the one-dimensional convection equation with constant velocity can be written as

$$\frac{\partial f}{\partial t} + u\frac{\partial f}{\partial x} = 0, \tag{2}$$

where $f(x, t)$ is the distribution function, $t \in [0, \infty)$ represents time, $x \in (-\infty, +\infty)$ is the space coordinate, and $u = \text{const}$ is the flow velocity. The solution of equation (2) can be constructed in the following way [*Evans*, 1998]:

$$f(x, t) = g(x - ut), \tag{3}$$

where g is an arbitrary smooth function.

The one-dimensional convection equation (2) can be completed with initial and boundary conditions to describe special physical cases. For instance, the solution of equation (2) with the initial condition

$$f(x, 0) = h(x), \tag{4}$$

where $h(x)$ is a known function, is

$$f(x, t) = h(x - ut). \tag{5}$$

If the one-dimensional convection equation (2) is considered on the interval $x \in [a, b]$, where $a, b < \infty$, and is complemented only with the periodic boundary conditions

$$f(a, t) = f(b, t), \tag{6}$$

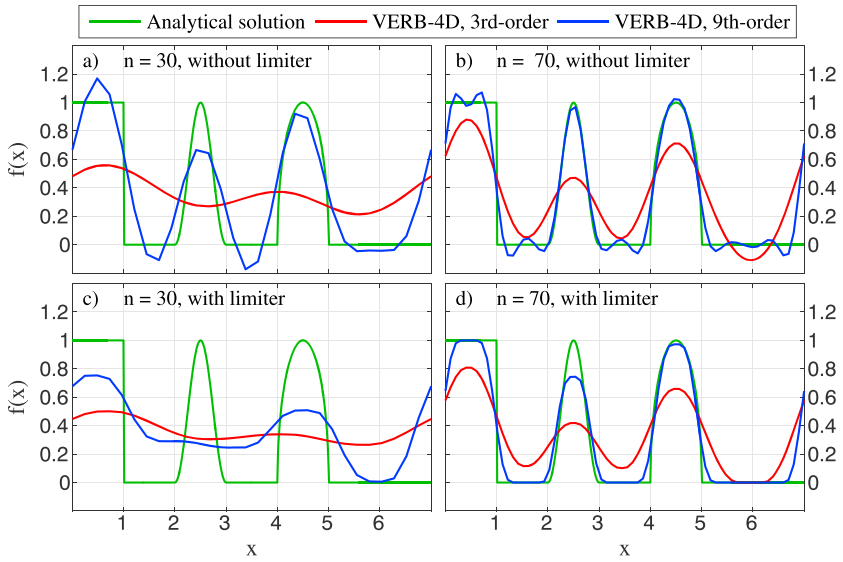

Figure 1. Comparison of the analytical solution (green line, from left to right: the step function, squared sine, and semiellipse) and VERB-4D solutions (third-order (red line) and ninth-order (blue line) schemes) of the one-dimensional convection equation for different grid sizes ((a and c) $n=30$ and (b and d) 70), with (Figures 1c and 1d) and without (Figures 1a and 1b) the universal limiter, $u=1$, $T=98$ (14 rotations).

the solution of equation (2) becomes

$$f(x,t) = \tilde{g}(x-ut), \tag{7}$$

where $\tilde{g}(\xi)$ is an arbitrary periodic function satisfying the following condition: $\tilde{g}(b-ut) = \tilde{g}(a-ut)$.

The choice of proper initial conditions in addition to the one-dimensional convection equation (2) allows us to validate a particular numerical scheme. The step function is a basic test of monotonicity (monotonic profiles should stay monotonic) and reproduction of discontinuities [*Leonard*, 1991]. One period of squared sine function represents a relatively smooth profile with a continuously turning gradient and single local maximum [*Leonard*, 1991; *Sweby*, 1984]. A semiellipse initial function [*Zalesak*, 1987] may force the numerical scheme to generate significant waviness near large gradients of the profile.

To test the block of the VERB-4D code modeling one-dimensional convection, let us consider the one-dimensional convection equation (2) with constant velocity and the periodic boundary conditions (6). In this set of tests we study the influence of spatial resolution on accuracy of results, unphysical oscillations generated by the high-order linear upwind schemes, and elimination of such oscillations using the universal limiter. We do not utilize here the discriminator decreasing the amplitude error near local extrema. The particular solution of the general form (7) can be specified by the choice of initial conditions. Using dimensionless parameters, we set velocity $u=1$ and left and right spatial boundaries $a=0$ and $b=7$, respectively. The initial profile consists of step function, squared sine, and semiellipse profiles. We run the VERB-4D code to calculate the profile at end time $T=98$ corresponding to 14 rotations of the profile (one rotation has the length $(b-a)$). Spatial grids contain $n=30$ and 70 nodes in our simulations. To guarantee the stability of the numerical scheme, we set up time step $\Delta t = 0.5\Delta x/u$ satisfying the Courant-Friedrichs-Lewy condition (see Appendix A), where Δx is the space step of the grid. Simulation results are shown in Figure 1.

Figure 1a depicts analytical and numerical solutions for grid size $n = 30$, if the universal limiter is not used. The green, red, and blue lines designate the analytical solution and numerical solutions obtained by using the third-order scheme and ninth-order scheme, respectively. The ninth-order scheme can reconstruct the general shape of sine and semiellipse while the shape of the step function is not yet reproduced. The violation of monotonicity is observed as negative values produced by the ninth-order numerical scheme. The third-order scheme has very strong numerical diffusion and is not able to reproduce even the general shape of the analytical profile. The application of the universal limiter (Figure 1c) eliminates unphysical nonmonotonic behavior, but considerable numerical diffusion becomes larger for both schemes. The increase of grid size to $n=70$

without using the universal limiter (Figure 1b) demonstrates almost perfect reconstruction of sine and semiellipse profiles for the ninth-order scheme. However, the profile experiences unphysical oscillations at constant values of the analytical solution. The third-order scheme still suffers from large amplitude error, numerical diffusion, and unphysical oscillations. The universal limiter removes oscillations (Figure 1d) for both third- and ninth-order schemes, though the limiter leads to the noticeable increase in the amplitude error of the sine function in the case of the ninth-order scheme. The amplitude error of the third-order scheme becomes even stronger as well.

Though the universal limiter allows us to use high-order schemes while avoiding unphysical oscillations, in some cases the limiter can introduce additional amplitude error. Other tests (not presented here) have shown that high-order schemes along with the universal limiter are more accurate than the lower order schemes utilizing the universal limiter and that higher velocities and longer times of calculation lead to less accurate results.

The presented test was performed for idealized one-dimensional profiles, constant velocity, and uniform spatial grid. Physics-based simulations may be more complicated, requiring variable velocities, logarithmic grid, and additional source or loss terms. The test may not be fully applicable at some energies, where particles are lost to the magnetopause or atmosphere in less than a few rotations, but they clearly illustrate the importance of an accurate numerical scheme.

3.2. Two-Dimensional Convection

The solution of the two-dimensional convection equation

$$\frac{\partial f}{\partial t} + u\frac{\partial f}{\partial x} + v\frac{\partial f}{\partial y} = 0, \tag{8}$$

where $f(x, y, t)$ is the required function, $t \in [0, \infty)$ represents time, $x, y \in (-\infty, +\infty)$ are space coordinates, and $u, v = \text{const}$ are velocities, can be generalized from the solution (3) of the one-dimensional convection equation (2):

$$f(x, y, t) = g(x - ut, y - vt), \tag{9}$$

where $g(\xi, \eta)$ is an arbitrary function.

Moreover, if equation (8) is completed with the factorized initial conditions

$$f(x, y, 0) = h_1(x)h_2(y), \tag{10}$$

where $h_1(\xi)$ and $h_2(\xi)$ are known functions, the solution of problem (8) is reduced to two one-dimensional problems (2) and (4) with $h(x) \equiv h_1(x)$ and $h_2(x)$ and can be found as follows:

$$f(x, y, t) = h_1(x - ut)h_2(y - vt). \tag{11}$$

The latter fact allows us to deduce analytical solutions for the two-dimensional convection equation on the basis of conclusions made for the one-dimensional equation.

As an example, we test here how significantly the numerical error depends on the order of the scheme and the duration of the simulation. We turn on the universal limiter and discriminator, aiming to study the realistic behavior of the profile. We impose the periodic boundary conditions in x and constant boundary conditions in y equaled 0 for two-dimensional convection equation (8). The periodic boundary conditions in x correspond to convection in MLT and constant boundary conditions in y correspond to convection in R. Initial conditions are factorized to two one-dimension profiles including step-function, squared sine, and semiellipse profiles. The computational domain is taken as a rectangle area $[0, 7] \times [0, 250]$ using dimensionless coordinates. The velocities in x and y are $u = 1$ and $v = 2$, respectively. Space steps in x and y are equal to 0.1. Time step is chosen using the same approach as for the one-dimensional test above.

The results of simulations are presented in Figures 2 and 3 for dimensionless end times $T = 7$ and 70, respectively. The analytical solutions are shown in Figures 2a, 2d, 3a and 3d for $T = 7$ and $T = 70$. The use of the ninth-order scheme (Figures 2e and 3e) results in smaller numerical diffusion than the use of the third-order scheme (Figures 2b and 3b). The differences between analytical and numerical solutions are shown in Figures 2c, 2f, 3c, and 3f. Figures 2c, 2f, 3c, and 3f show significant numerical errors close to the step function

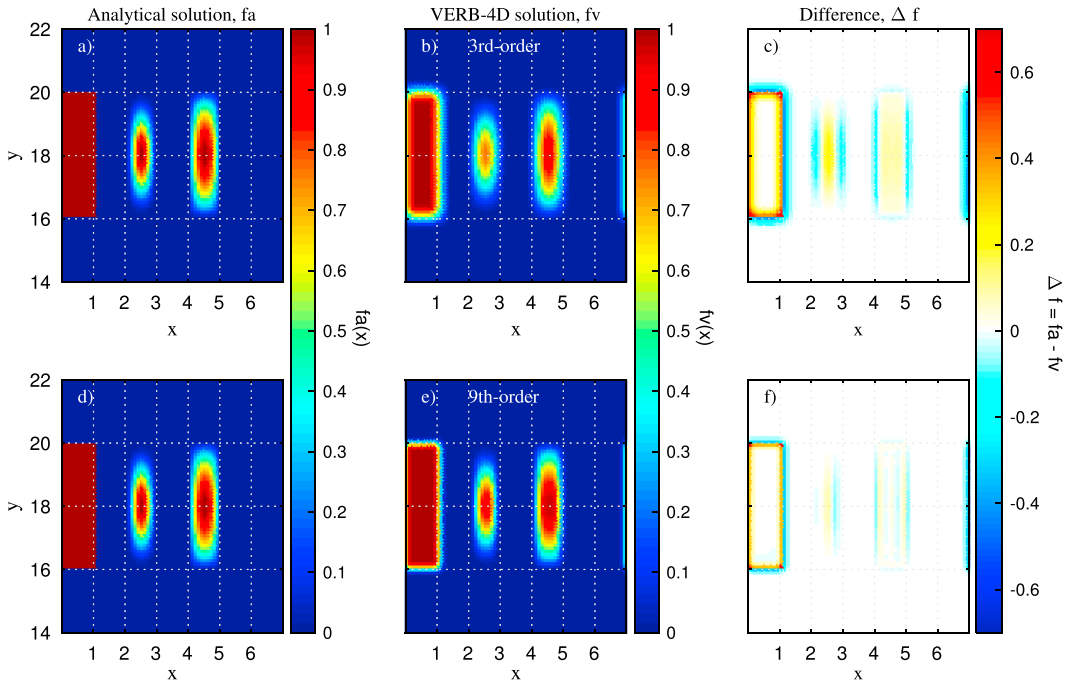

Figure 2. Comparison of the (a and d) analytical solution and VERB-4D solutions ((b) third-order and (e) ninth-order schemes) of the two-dimensional convection equation and differences between analytical solution and each (c and f) numerical solution for end time **T** = **7** (1 rotation in x), $u = 1$, $v = 2$, and space steps in x and y equaled 0.1. Step, squared sine, and semiellipse are depicted at each plot from left to right.

in all considered cases. In the case of the third-order scheme, sine and semiellipse profiles obtained numerically also show numerical errors comparable with the error on the edges of the step function. Numerical error on the edges of sine and semiellipse profiles predominantly appears in x direction (Figures 2c and 2f and 3c and 3f), since gradients in y direction are smaller and numerical diffusion in y is weaker, leading to lower error.

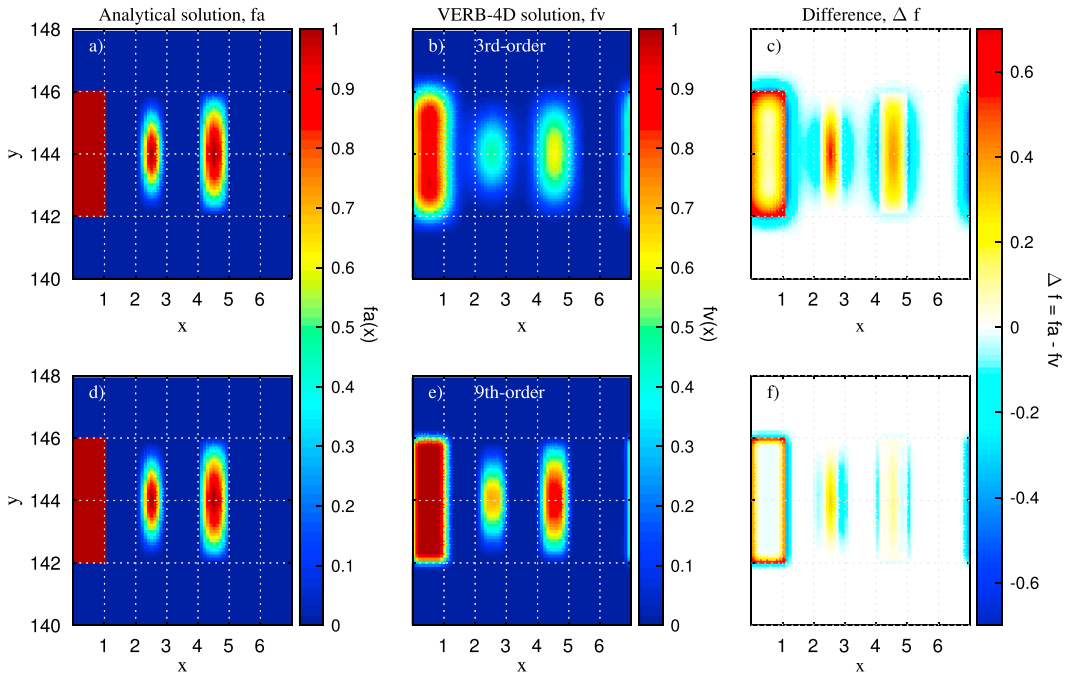

Figure 3. Same as Figure 2 but for longer end time $T = 70$.

For longer computational times, the errors accumulate due to inaccuracies of time and space discretization and increase.

3.3. One-Dimensional Diffusion and Two-Dimensional Diffusion With Mixed Terms

Now let us consider the one-dimensional diffusion equation with constant diffusion coefficient $D > 0$:

$$\frac{\partial f}{\partial t} - D\frac{\partial^2 f}{\partial x^2} = 0, \tag{12}$$

where $f(x,t)$ is the required function, $t \in [0, +\infty)$ is time, and $x \in (-\infty, +\infty)$ is a space coordinate. If we take a Gaussian with a nonzero parameter σ as an initial condition

$$f(x,0) = e^{-x^2/2\sigma}, \tag{13}$$

the solution of equation (12) is represented in the form of a widening Gaussian [*Strang*, 2007]:

$$f(x,t) = \frac{1}{\sqrt{1+2Dt/\sigma}} e^{-x^2/(2\sigma+4Dt)}. \tag{14}$$

A Gaussian (13) is appropriate for investigation of numerical scheme on smooth solutions, since it is infinitely differentiable.

To explore the behavior of a numerical scheme on discontinuous functions, it is convenient to set the initial conditions in addition to one-dimensional diffusion equation (12) as a step function:

$$f(x,0) = \begin{cases} 1, & |x| < x_0, \\ 0, & |x| > x_0, \end{cases} \tag{15}$$

where x_0 is a known number. In this case, the analytical solution can be found in the following form [*Polyanin*, 2001]:

$$f(x,t) = \frac{1}{2}\left[\operatorname{erf}\left(\frac{x_0 - x}{2\sqrt{Dt}}\right) + \operatorname{erf}\left(\frac{x_0 + x}{2\sqrt{Dt}}\right)\right], \tag{16}$$

where

$$\operatorname{erf}(x) = \frac{2}{\sqrt{\pi}} \int_0^x e^{-\tilde{x}^2} \mathrm{d}\tilde{x}. \tag{17}$$

All conclusions relating to the one-dimensional diffusion problem can be generalized in the case of the two-dimensional diffusion equation with constant diffusion coefficients D_{xx} and D_{yy}

$$\frac{\partial f}{\partial t} - D_{xx}\frac{\partial^2 f}{\partial x^2} - D_{yy}\frac{\partial^2 f}{\partial y^2} = 0. \tag{18}$$

We solve (18) for $t \in [0, +\infty)$, $x, y \in (-\infty, +\infty)$, $D_{xx}, D_{yy} > 0$. This generalization can be demonstrated by introducing factorized initial conditions for equation (18):

$$f(x,y,0) = f_1(x) f_2(y), \tag{19}$$

where $f_1(x)$ and $f_2(y)$ are known functions. The solution of problem (18) with initial condition (19) is also factorized to solutions $f_1(x,t)$ and $f_2(y,t)$ of the corresponding one-dimensional diffusion equations in each space coordinate with constant positive diffusion coefficients D_{xx} and D_{yy}:

$$f(x,y,t) = f_1(x,t) f_2(y,t). \tag{20}$$

To obtain the analytical form of the solution, one can use either the widening Gaussian (14) or function (16) as $f_1(x,0) \equiv f_1(x)$ and $f_2(y,0) \equiv f_2(y)$.

It is also customary to obtain the analytical solution for the two-dimensional diffusion equation with mixed terms. Assuming constant diffusion coefficients D_{xx}, $D_{xy} = D_{yx}$, and D_{yy}, the equation takes the form

$$\frac{\partial f}{\partial t} - D_{xx}\frac{\partial^2 f}{\partial x^2} - D_{yy}\frac{\partial^2 f}{\partial y^2} - 2D_{xy}\frac{\partial^2 f}{\partial x \partial y} = 0, \tag{21}$$

where $t \in [0, +\infty)$, $x, y \in (-\infty, +\infty)$, $D_{xx}, D_{yy} > 0$, and $D_{xx}D_{yy} > D_{xy}^2$.

The mixed diffusion term D_{xy} in (21) can be eliminated using the following technique [*Albert and Young*, 2005]. Applying the linear transformation of coordinates $(x, y) \rightarrow (\xi, \eta)$

$$\xi = ax + by, \eta = cx + dy, \tag{22}$$

where $ad - bc \neq 0$, diffusion coefficients in new coordinates can be written as [*Haerendel*, 1968; *Schulz and Lanzerotti*, 1974]

$$\begin{aligned} D_{\xi\xi} &= a^2 D_{xx} + 2abD_{xy} + b^2 D_{yy}, \\ D_{\eta\eta} &= c^2 D_{xx} + 2cdD_{xy} + d^2 D_{yy}, \\ D_{\xi\eta} &= acD_{xx} + (ad + bc)D_{xy} + bdD_{yy}. \end{aligned} \tag{23}$$

The diffusion coefficient $D_{\xi\eta}$ can be eliminated, if the following condition is satisfied:

$$acD_{xx} + (ad + bc)D_{xy} + bdD_{yy} = 0. \tag{24}$$

The positivity of $D_{\xi\xi}$ and $D_{\eta\eta}$ is guaranteed by the inequality $D_{xx}D_{yy} > D_{xy}^2$.

The diffusion equation with mixed terms (21) can be simplified to equation (18) with corresponding diffusion coefficients $D_{\xi\xi}$ and $D_{\eta\eta}$, if D_{xx}, D_{yy} and D_{xy} in equation (21) satisfy the restriction (24). Therefore, an analytical solution of the diffusion equation (18) without mixed terms can be used for the construction of an analytical solution of the two-dimensional diffusion equation (21) with mixed terms. For instance, if the initial conditions for (21) is the following function with positive parameters σ_1 and σ_2

$$f(x, y, 0) = e^{-(ax+by)^2/2\sigma_1} e^{-(cx+dy)^2/2\sigma_2}, \tag{25}$$

the solution of problem (21) can be found as follows:

$$\begin{aligned} f(x, y, t) = &\left[1 + 2\frac{\left(a^2 D_{xx} + 2abD_{xy} + b^2 D_{yy}\right) t}{\sigma_1}\right]^{-\frac{1}{2}} \times \left[1 + 2\frac{\left(c^2 D_{xx} + 2cdD_{xy} + d^2 D_{yy}\right) t}{\sigma_2}\right]^{-\frac{1}{2}} \\ &\times e^{-(ax+by)^2/\left(2\sigma_1 + 4\left(a^2 D_{xx} + 2abD_{xy} + b^2 D_{yy}\right)t\right)} \times e^{-(cx+dy)^2/\left(2\sigma_2 + 4\left(c^2 D_{xx} + 2cdD_{xy} + d^2 D_{yy}\right)t\right)} \end{aligned} \tag{26}$$

for all a, b, c, and d satisfying (24) and $ad - bc \neq 0$.

Our next set of tests is devoted to the investigation of the convergence of the numerical solution of the two-dimensional diffusion equation (21) with mixed terms to the analytical solution. We set $D_{xx} = D_{yy} = 10$ and $D_{xy} = 7$, using dimensionless units to satisfy the condition $D_{xx}D_{yy} > D_{xy}^2$. The function (25) with parameters $a = c = d = 1/\sqrt{2}$, $b = -1/\sqrt{2}$, $\sigma_1 = \sigma_2 = 200$ is chosen as the initial condition for equation (21). Note that the chosen parameters a, b, c, and d along with the diffusion coefficients D_{xx}, D_{yy}, D_{xy} satisfy condition (24). Zero values of the required function are chosen as constant boundary conditions at infinities. To emulate spatial infinities, we use square $[-200, 200] \times [-200, 200]$ since the sizes of the square are considerably larger than the characteristic size of the initial function, and the required function can be approximated with zero at the borders of the square.

Figure 4 represents analytical solutions (Figures 4a, 4d, and 4g), numerical solutions (Figures 4b, 4e, and 4h), and their differences (Figures 4c, 4f, and 4i) for grid sizes 25×25, 50×50, and 100×100 for the end time $T = 70$ and the time step 0.14. The VERB-4D solutions represent anisotropic diffusion in (ξ, η) coordinates (22) rotated 45° clockwise about (x, y) axes. Indeed, diffusion with mixed terms in (x, y) coordinates is equivalent to anisotropic diffusion without mixed terms in (ξ, η) coordinates, since $D_{\xi\xi} = 3$, $D_{\eta\eta} = 17$, and $D_{\xi\eta} = 0$ (see equations (23)). Numerical errors have the same shape in all cases (Figures 4c, 4f, and 4i). The VERB-4D solution underestimates the analytical one along the line $y = x$ and overestimates it along the lines $y = x \pm 50$. The absolute difference decreases about 3.5 times when the space step decreases 2 times in each variable. Therefore, a numerical solution of the VERB-4D code converges to the analytical solution.

As expected, further tests (not presented here) showed stability of numerical solution to an increasing time step, since the implemented numerical scheme for the two-dimensional diffusion with mixed terms is fully implicit.

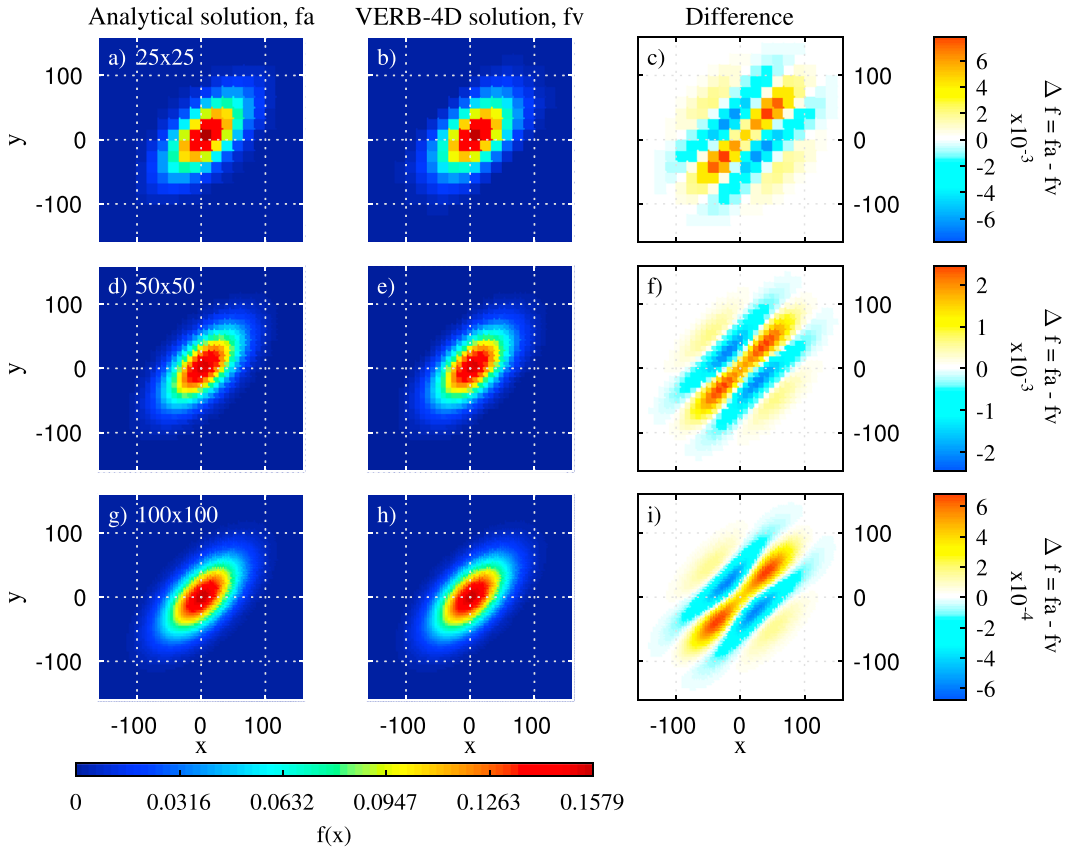

Figure 4. Comparison of (a, d, and g) analytical solution and (b, e, and h) VERB-4D solution of the two-dimensional diffusion equation with mixed terms and (c, f, and i) their difference for grid sizes 25×25, 50×50, and 100×100, $x \in [-200, 200]$, $y \in [-200, 200]$, $T = 70$, $D_{xx} = D_{yy} = 10$, $D_{xy} = 7$, $\sigma = 200$.

4. Influence of Numerical Schemes on Magnetospheric Convection Modeling

We performed a set of simulations in order to investigate the influence of the order of the scheme for the convection equation on magnetospheric convection modeling. Here we turn on the universal limiter and the discriminator, which are applied to the third- and ninth-order schemes. We assign diffusion coefficients $\langle D_{L^*L^*} \rangle$, $\langle D_{VV} \rangle$, $\langle D_{VK} \rangle$, $\langle D_{KV} \rangle$, and $\langle D_{KK} \rangle$ in the Fokker-Planck equation (1) to zero and take into account only convection terms and losses due to magnetopause shadowing based on the Shue model [*Shue et al.*, 1997]. The computational domain in R and φ is set as a rectangle in polar coordinates $[6.6R_E, 10R_E] \times [0, 2\pi]$. Boundary conditions in φ are periodic. Zero derivative boundary conditions are used at 6.6 R_E. Constant boundary conditions at $R = 10$ R_E are parameterized using kappa function with $\kappa = 3.3$, the electron density taken from *Tsyganenko and Mukai* [2003], and the parameterization of electron temperature provided by [N. Ganushkina, personal communication, 2015]. An empty magnetosphere is taken as initial conditions. Azimuthal and radial velocities $\langle v_\varphi \rangle$ and $\langle v_R \rangle$ are calculated using the centered dipole approximation and the Volland-Stern electric field model [*Volland*, 1973; *Stern*, 1975] with the *Kp*-dependent intensity according to *Maynard and Chen* [1975].

To study an impact of the numerical scheme on the results of magnetospheric convection modeling, we assume quiet time geomagnetic conditions ($Kp = 2$, IMF $B_z = 0$ nT, solar wind number density is equal to 7 cm^{-3}, and solar wind velocity is equal to 400 km/s). Several pulses of localized electric field are launched, as described below, to investigate the response of different numerical schemes to sharp changes in velocities and PSD. The localized electric field is associated with the dipolarization process in the magnetosphere [*Baumjohann et al.*, 1990; *Angelopoulos et al.*, 1992]. Propagating in the eastward direction, electromagnetic

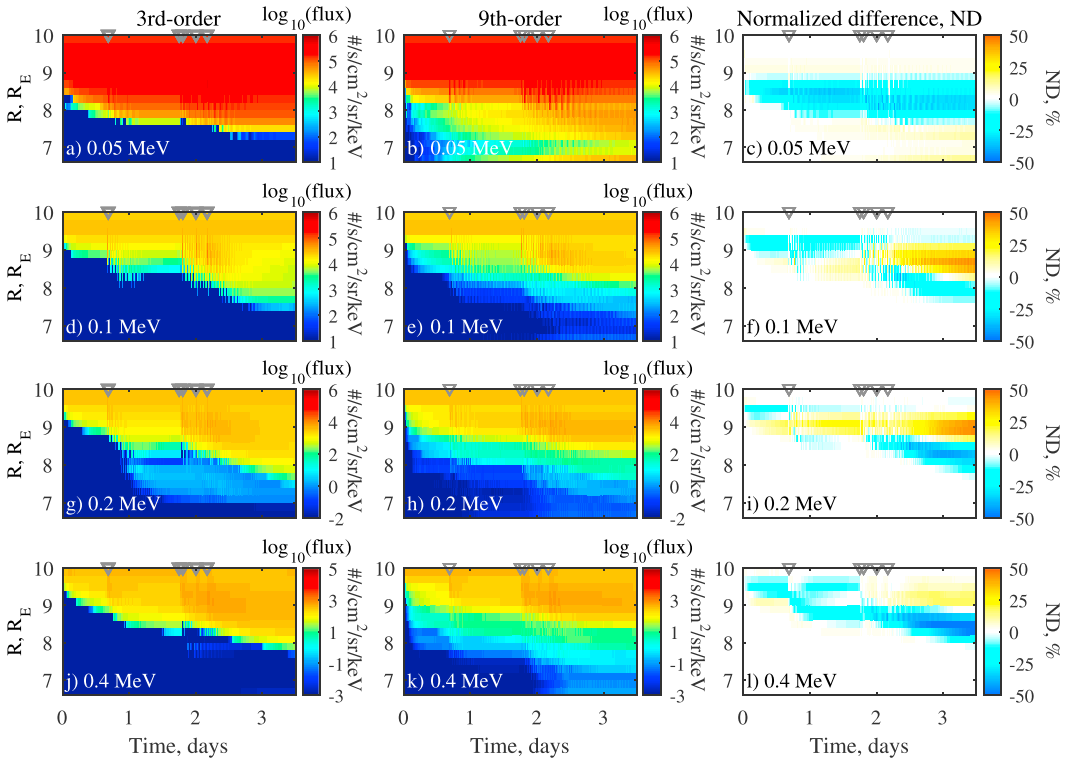

Figure 5. Electron fluxes obtained by using the (a, d, g, and j) third-order and (b, e, h, and k) ninth-order schemes and the (c, f, i, and l) normalized difference for 50° pitch angle, MLT = 3. Times of arrival of localized electric field are marked with gray triangles.

pulses are calculated following *Li et al.* [1998] and *Sarris et al.* [2002]. In the spherical coordinate system, the localized electric field takes the form

$$\mathbf{E}_{\phi} = -\hat{e}_{\phi} E_0 / E_{\max} \left(1 + c_1 \cos(\phi - \phi_0)\right)^p \exp(-\xi^2), \tag{27}$$

where $\hat{e}_{\phi}$ is the unit vector in the direction of the increase of azimuth angle ϕ (MLT coordinate φ and the azimuth angle ϕ can differ in the direction of increase and can be shifted by phase relative to each other, but in general, they have almost the same meaning), $\xi = [r - r_i + v(r)(t - t_a)]/d$ is the location of the maximum intensity of the pulse, $v(r) = a + br$ describes the pulse front velocity as a function of radial distance r, d is the width of the pulse, $c_1 > 0$ and $p > 0$ are coefficients determining the local time dependence of the electric field amplitude, $t_a = \left(c_2 / v_a\right)\left(1 - \cos(\phi - \phi_0)\right)$ represents the delay of the pulse depending on the azimuth angle, ϕ_0 is the azimuth angle of the fastest transport to given r, c_2 is the magnitude of the delay, v_a is the longitudinal speed of the pulse, and r_i is a parameter affecting the arrival time of the pulse. The parameter $E_{\max}$ is introduced to eliminate unphysical values in excess of 1000 mV/m for the maximum E_{ϕ} according to *Ganushkina et al.* [2006]. Following *Sarris et al.* [2002], we use $\phi_0 = 0$, $c_1 = 1$, $c_2 = 0.5\ R_E$, $a = 53.15$ km/s, $b = 0.0093\ \mathrm{s}^{-1}$, $p = 8$, $v_a = 20$ km/s, $r_i = 100\ R_E$, $d = 4 \cdot 10^7$ m, and $E_0 = 4$ mV/m.

The evolution of PSD is calculated for 3.5 days. The launched electric field pulses reach the computational domain at $t = 0.68$, 1.76, 1.8, 2.01, and 2.18 days. Space step is equal to $0.2\ R_E$ in R and $\pi/6$ in φ, corresponding to the spatial grid in R and φ of the size of 18×13.

Figure 5 represents evolution of fluxes in time for different R calculated with the third- and ninth-order schemes for 0.05, 0.1, 0.2, and 0.4 MeV electrons. Figures 5a, 5d, 5g, and 5j depict fluxes obtained with the third-order upwind scheme, and Figures 5b, 5e, 5h, and 5k show electron fluxes calculated using the ninth-order scheme. To compare these results for particular energies, we introduce the normalized differences (ND) metric [*Subbotin and Shprits*, 2009]:

$$\mathrm{ND} = \frac{f_{9\mathrm{th}}(t,R) - f_{3\mathrm{rd}}(t,R)}{\max\limits_{\text{over R for fixed t}} \left(f_{3\mathrm{rd}}(t,R) + f_{9\mathrm{th}}(t,R)\right)/2} \times 100\%, \tag{28}$$

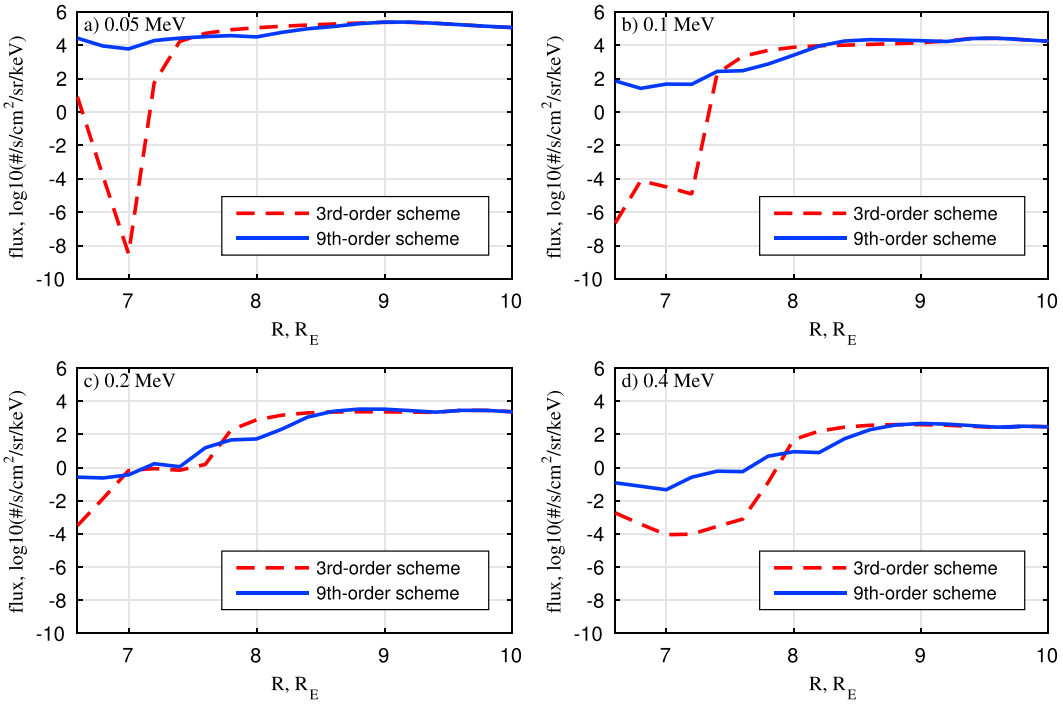

Figure 6. Dependence of numerically calculated profiles of electron fluxes on the scheme order for a simulation at t = 3 day, MLT =3, pitch angle $\alpha = 50°$. (a–d) Electron energies E = 0.05, 0.1, 0.2, and 0.4 MeV, respectively. The dashed line denotes results obtained with the third-order scheme, and the solid line depicts the results obtained with the ninth-order scheme.

where f_{3rd} and f_{9th} are PSD (or fluxes) modeled on the basis of the third- and ninth-order schemes. Figures 5c, 5f, 5i, and 5l depict normalized difference for energies E under consideration. Times of arrival of localized electric field are marked with gray triangles at the top of each plot. Considerable differences, about 50% in terms of the ND metric, appear after the third day at $R \approx 8.5\,R_E$ for 0.1 MeV electrons and at $R \approx 9\,R_E$ for 0.2 MeV electrons, where the ninth-order scheme results in more prominent flux than the third-order one. On the contrary, the third-order scheme gives higher fluxes for 0.4 MeV particles at $R \approx 8.4\,R_E$, where the normalized difference is equal to about −50%. The ND of the order of −(25–35)% at $R \approx 8–9\,R_E$ characterizes results for 0.05 MeV particles during the whole interval of calculations.

It is instructive to compare the resultant profiles at the end of the third day of the simulation (Figure 6). Both schemes show approximately the same results at $R \approx 9–10\,R_E$. The difference becomes more pronounced at lower radial distances. Fluxes obtained with the ninth-order scheme are up to 1 order lower at $8 \pm 0.5\,R_E$ for all energies. The ninth-order scheme gives significantly higher results at the lowest R (below 7.5 R_E for E = 0.05 and E = 0.1 MeV, below 7 R_E for E = 0.2 MeV, and below 8 R_E for E = 0.4 MeV).

To conclude, the ninth-order scheme leads to higher fluxes in comparison with the third-order scheme below $R \approx 8\,R_E$ at the end of the calculation. It can therefore be said that the ninth-order scheme results in faster transport of electrons to lower R. Though we have not compared results of the simulation with observations in this study, we can rely on the ninth-order scheme, as the scheme shows more accurate results and better reproduces the analytical solutions (see section 3).

5. Summary and Conclusions

Presented numerical simulations show the importance of detailed stability and accuracy verification tests for the inner magnetospheric models. Numerical instabilities may produce inadequate results and render the code unusable. Violation of accuracy can lead to more intricate issues, when numerical errors and uncertainties of physical models are indistinguishable, or may lead to erroneous physical conclusions or estimation of the missing physics. Low-accuracy numerical schemes require a finer grid than the more accurate schemes to

achieve the same results and consequently have a negative impact on the performance of the code. For these reasons, the validation of numerical schemes is an essential stage before the validation of the code with data.

In this work, we presented a set of convenient analytical solutions and verification tests for advective-diffusive codes. Accuracy and stability of numerical schemes for the inner magnetosphere modeling can be studied, choosing the appropriate initial and boundary conditions and comparing the simulation results with analytical solutions. Though the presented analytical profiles are constructed under strong assumptions such as constant velocities or constant diffusion coefficients, the basic behavior of implemented numerical schemes can be investigated using both smooth and discontinuous solutions.

We performed a comprehensive analysis of numerical methods and techniques underlying the VERB-4D code. Below is the list of the main findings:

1. It is crucially important to use accurate numerical schemes in the inner magnetospheric models. Our simulations have shown (Figures 5 and 6) that accuracy of numerical schemes significantly affects simulation results of an advective code.
2. Low-order numerical schemes for the convection equation can lead to large errors. For instance, the third-order scheme results in stronger numerical dissipation and a higher amplitude error than the ninth-order one (Figures 1–3).
3. Our tests of the convection and diffusion solvers implemented in the VERB-4D code have shown the convergence of the numerical solution to the analytical one.
4. The VERB-4D code demonstrates stable behavior independently of the input time step.

Appendix A: Courant-Friedrichs-Lewy Condition

Stability of numerical schemes is a key aspect in the construction of robust methods for solving partial differential equations. Unstable schemes can magnify small inaccuracies of initial conditions or numerical solutions, resulting in a large total numerical error and rendering even high-order schemes inapplicable for complex physical problems. Stable schemes can be either conditionally or unconditionally stable. As the name implies, unconditionally stable schemes are stable for any parameters of modeled system and numerical methods (i.e., velocity and space step), while conditionally stable schemes restrict these parameters.

We present here the simplest condition for a wide class of schemes for solving one-dimensional convection equation, the Courant-Friedrichs-Lewy condition [*Godunov and Ryabenkii*, 1987]. We consider equation (2) with constant positive velocity u. Assume that spatial boundary is confined by interval $[a, b]$. Then, we introduce a uniform spatial grid $\{x_i\}_{i=1}^{N_x}, x_i = a + (i-1)\cdot\Delta x, \Delta x = (b-a)/(N_x-1), i = 1, \ldots, N_x$. Time discretization is performed at moments $t_n = n\cdot\Delta t$. Discrete values of required function are denoted as $f(x_i, t_n) = f_i^n$.

The first-order explicit conditionally stable scheme for one-dimensional convection equation (2) can be written as follows:

$$\frac{f_i^{n+1} - f_i^n}{\Delta t} + u\frac{f_i^n - f_{i-1}^n}{\Delta x} = 0. \tag{A1}$$

The scheme (A1) is stable if the following condition is satisfied:

$$\frac{u\Delta t}{\Delta x} \le 1. \tag{A2}$$

Condition (A2) is called the Courant-Friedrichs-Lewy (CFL) condition, and the number $c = u\Delta t/\Delta x$ is called the Courant number. The CFL condition is also valid for more accurate high-order schemes and can be generalized for equations with variable velocities. If low-order schemes, requiring small space steps for high accuracy, are used, relatively small time steps should inevitably be utilized. In this case, computational time may be increased significantly, which particularly has a negative impact on long-term simulations.

Appendix B: Elimination of Unphysical Oscillations Using the Universal Limiter

Following, in general, *Leonard* [1991], we briefly describe the method of the construction of high-order numerical schemes for the one-dimensional convection equation (2), free of unphysical oscillations. Equation (2) is considered at the spatial domain $[a, b]$ and the time interval $[0, +\infty)$. For generality, the velocity $u = u(x, t)$

Table B1. Coefficients for Calculation $2 \cdot D^{n,(N)}_{i+1/2}$

N	a_5	a_4	a_3	a_2	a_1	a_0	a_{-1}	a_{-2}	a_{-3}	a_{-4}
0	0	0	0	0	+1	+1	0	0	0	0
1	0	0	0	+1	0	−1	0	0	0	
2	0	0	0	+1	−1	−1	+1	0	0	0
3	0	0	+1	−2	0	+2	−1	0	0	
4	0	0	+1	−3	+2	+2	−3	+1	0	0
5	0	+1	−4	+5	0	−5	+4	−1	0	
6	0	+1	−5	+9	−5	−5	+9	−5	+1	0
7	+1	−6	+14	−14	0	+14	−14	+6	−1	
8	+1	−7	+20	−28	+14	+14	−28	+20	−7	+1
…	…	…	…	…	…	…	…	…	…	…

is assumed to be variable in both space and time. The spatial domain is uniformly divided into N_x nodes: $x_i = a + (i-1)\cdot\Delta x$, $i = 1, \ldots, N_x$. The required function is considered at the nodes $\{x_i\}_{i=1}^{N_x}$ and calculated at discrete times $t_n = n\cdot\Delta t$: $f(x_i, t_n) = f_i^n$, $n = 1, \ldots$

The value of the function at the node x_i and the moment t_{n+1} can be represented as follows:

$$f_i^{n+1} = f_i^n - \left(c^n_{i+1/2} f^n_{i+1/2} - c^n_{i-1/2} f^n_{i-1/2}\right), \tag{B1}$$

where $c^n_{i\pm1/2} = u(x_i \pm \Delta x/2, t_n)\Delta t/\Delta x$ is the Courant number and $f^n_{i\pm1/2} = f(x_i \pm \Delta x/2, t_n)$. Since the discretized function $f(x,t)$ is defined only at the nodes x_i, the values $f^n_{i\pm1/2}$ have to be approximated on the basis of known values f_i^n.

The value of $f^n_{i+1/2}$ for the arbitrary odd Nth order ($N > 1$) upwind scheme satisfies the recursive expression

$$f^{n,(N)}_{i+1/2} = f^{n,(N-1)}_{i+1/2} + \frac{\prod_{k=1}^{(N-1)/2}\left(\left(c^n_{i+1/2}\right)^2 - k^2\right)}{N!}\left[D^{n,(N-1)}_{i+1/2} - \frac{\mathrm{sign}\left(c^n_{i+1/2}\right)}{2}\delta^{n,(N)}_{i+1/2}\right], \tag{B2}$$

where $f^{n,(N)}_{i+1/2}$ is the value of $f^n_{i+1/2}$ corresponding to the Nth order scheme, $f^{n,(0)}_{i+1/2} = \frac{1}{2}(f^n_{i+1} + f^n_i)$, $\mathrm{sign}(c^n_{i+1/2})$ is the sign of the Courant number, and coefficients $D^{n,(N-1)}_{i+1/2}$ and $\delta^{n,(N)}_{i+1/2}$ can be expanded into the following sums:

$$D^{n,(N-1)}_{i+1/2} = \frac{1}{2}\sum_j a_j f^n_{i+j}, \tag{B3}$$

$$\delta^{n,(N)}_{i+1/2} = \sum_j b_j f^n_{i+j} \tag{B4}$$

with finite number of nonzero coefficients a_j and b_j. Values of a_j and b_j can be obtained from Tables B1 and B2.

In case of even $N > 2$, $f^n_{i+1/2}$ can be approximated as follows:

$$f^{n,(N)}_{i+1/2} = f^{n,(N-2)}_{i+1/2} + \frac{\prod_{k=1}^{N/2-1}\left(\left(c^n_{i+1/2}\right)^2 - k^2\right)}{(N-1)!}\left[D^{n,(N-2)}_{i+1/2} - \frac{c^n_{i+1/2}}{N}\delta^{n,(N-1)}_{i+1/2}\right]. \tag{B5}$$

Utilizing expressions (B2) and (B5) together with (B1), one can calculate the evolution of the required function from the moment t_n to t_{n+1}.

It is well known that high-order (higher than second order) linear numerical schemes for the one-dimensional convection equation suffer from artificial unphysical oscillations [*Godunov*, 1959]. *Leonard* [1991] developed the universal limiter eliminating unphysical oscillations. The universal limiter is applicable to a numerical

Table B2. Coefficients for Calculation $\delta^{n,(M)}_{i+1/2}$

M	b_5	b_4	b_3	b_2	b_1	b_0	b_{-1}	b_{-2}	b_{-3}	b_{-4}
0		0	0	0	0	+1	0	0	0	0
1	0	0	0	0	+1	−1	0	0	0	0
2		0	0	0	+1	−2	+1	0	0	0
3	0	0	0	+1	−3	+3	−1	0	0	0
4		0	0	+1	−4	+6	−4	+1	0	0
5	0	0	+1	−5	+10	−10	+5	−1	0	0
6		0	+1	−6	+15	−20	+15	−6	+1	0
7	0	+1	−7	+21	−35	+35	−21	+7	−1	0
8		+1	−8	+28	−56	+70	−56	+28	−8	+1
9	+1	−9	+36	−84	+126	−126	+84	−36	+9	−1
…	…	…	…	…	…	…	…	…	…	…

scheme of arbitrary order. The limiter is based on the three stages: (i) calculation $f^n_{i+1/2}$ using (B2) and (B5) for all i, (ii) modification of $f^n_{i+1/2}$ if unphysical oscillations are detected, and (iii) updating f^n_i according to (B1). Details of the universal limiter are presented in the following algorithm.

1. Set $i = 1$.
2. While $i \le N_x$ do
   (a) if $c^n_{i+1/2} = 0$: set $i \to i+1$ and go to step 2;
   (b) calculate $f^n_{i+1/2}$ for the desired order scheme using (B2) and (B5);
   (c) among adjacent to $x_i + \Delta x/2$ nodes x_j designate nearest upstream (C), next to the nearest upstream (U), and nearest downstream (D) nodes on the basis of sign $\left(c^n_{i+1/2}\right)$;
   (d) compute DEL $= f^n_D - f^n_U$ and ADEL $= |$DEL$|$;
   (e) compute ACURV $= |f^n_D - 2f^n_C + f^n_U|$;
   (f) if ACURV $\ge$ ADEL: set $f^n_{i+1/2} \to f^n_C$; $i \to i+1$; go to step 2;
   (g) compute the reference value $f_{\text{ref}} = f^n_U + \left(f^n_C - f^n_U\right)/c^n_{i+1/2}$;
   (h) if DEL > 0: $f^n_{i+1/2} \to \max\left(f^n_{i+1/2}, f^n_C\right)$; $f^n_{i+1/2} \to \min\left(f^n_{i+1/2}, \min\left(f_{\text{ref}}, f^n_D\right)\right)$;
   (i) else $f^n_{i+1/2} \to \min\left(f_{\text{ref}}, f^n_C\right)$; $f^n_{i+1/2} \to \max\left(f^n_{i+1/2}, \max\left(f_{\text{ref}}, f^n_D\right)\right)$;
   (j) $i \to i+1$;
   (k) go to step 2
3. Update the function f^n_i for all i according to expression (B1).

The universal limiter can produce slight amplitude error near points of local extrema, where changes in monotonicity are mistakenly recognized as short wavelength unphysical oscillations. The discriminator proposed by *Leonard and Niknafs* [1991] analyzes the behavior of the function near each node x_i and decides, on the basis of value and sign of gradient at the adjacent nodes, if the associated oscillation relates to local extrema. If local extrema is detected, the discriminator relaxes the universal limiter constraints, and stages 2c-2i of the algorithm above are skipped.

Finally, we note that if formulas (B2) and (B5) are used near the boundaries of the spatial domain $[a, b]$, the expansions (B3) and (B4) may require values of f^n_i beyond the range $i = 1, \ldots, N_x$ (e.g., f^n_{-1} and $f^n_{N_x+1}$). In this case, the necessary number of "ghost" points has to be introduced in accordance with the order of the desired numerical scheme. Values of the function $f(x, t)$ at these points should be chosen depending on the type of boundary conditions.

Acknowledgments
This project received funding support from NASA grant NNX15AI94G, NSF grant AGS-1203747, and the UC Office of the President, UC Lab Fees Research Program Award ID 12-LR-235337. We would like to thank Dmitri Subbotin for his contributions to the development of the VERB-4D code. We would like to thank Natalia Ganushkina for providing parameterization of electron temperature. We would like to thank the anonymous reviewers for their insightful comments and suggestions that have contributed to improve this paper. No data was used in producing this manuscript.

References

Albert, J., and S. Young (2005), Multidimensional quasi-linear diffusion of radiation belt electrons, *Geophys. Res. Lett.*, *32*(14), L14110, doi:10.1029/2005GL023191.

Anderson, E., et al. (1999), *LAPACK Users' Guide*, 3rd edn., vol. 9, SIAM Philadelphia, Philadelphia, Pa.

Angelopoulos, V., W. Baumjohann, C. Kennel, F. Coroniti, M. Kivelson, R. Pellat, R. Walker, H. Lühr, and G. Paschmann (1992), Bursty bulk flows in the inner central plasma sheet, *J. Geophys. Res.*, *97*(A4), 4027–4039, doi:10.1029/91JA02701.

Axford, W. (1969), Magnetospheric convection, *Rev. Geophys.*, *7*(1–2), 421–459, doi:10.1029/RG007i001p00421.

Baker, D., S. Kanekal, X. Li, S. Monk, J. Goldstein, and J. Burch (2004), An extreme distortion of the Van Allen belt arising from the Halloween solar storm in 2003, *Nature*, *432*(7019), 878–881, doi:10.1038/nature03116.
Baumjohann, W., G. Paschmann, and H. Lühr (1990), Characteristics of high-speed ion flows in the plasma sheet, *J. Geophys. Res.*, *95*(A4), 3801–3809, doi:10.1029/JA095iA04p03801.
Beutier, T., and D. Boscher (1995), A three-dimensional analysis of the electron radiation belt by the Salammbô code, *J. Geophys. Res.*, *100*(A8), 14,853–14,861, doi:10.1029/94JA03066.
Brautigam, D., and J. Albert (2000), Radial diffusion analysis of outer radiation belt electrons during the October 9, 1990, magnetic storm, *J. Geophys. Res.*, *105*(A1), 291–309, doi:10.1029/1999JA900344.
Craven, J. (1966), Temporal variations of electron intensities at low altitudes in outer radiation zone as observed with satellite Injun 3, *J. Geophys. Res.*, *71*(23), 5643–5663, doi:10.1029/JZ071i023p05643.
Drozdov, A., Y. Shprits, K. Orlova, A. Kellerman, D. Subbotin, D. Baker, H. Spence, and G. Reeves (2015), Energetic, relativistic, and ultrarelativistic electrons: Comparison of long-term VERB code simulations with Van Allen Probes measurements, *J. Geophys. Res. Space Physics*, *120*(5), 3574–3587, doi:10.1002/2014JA020637.
Dungey, J. (1961), Interplanetary magnetic field and the auroral zones, *Phys. Rev. Lett.*, *6*(2), 47–48, doi:10.1103/PhysRevLett.6.47.
Elkington, S., M. Hudson, and A. Chan (2003), Resonant acceleration and diffusion of outer zone electrons in an asymmetric geomagnetic field, *J. Geophys. Res.*, *108*(A3), 1116, doi:10.1029/2001JA009202.
Evans, L. (1998), *Partial Differential Equations*, Graduate Studies in Math, vol. 19, American Mathematical Society, Providence, R. I.
Falthammar, C.-G. (1965), Effects of time-dependent electric fields on geomagnetically trapped radiation, *J. Geophys. Res.*, *70*(11), 2503–2516, doi:10.1029/JZ070i011p02503.
Fennell, J., S. Claudepierre, J. Blake, T. O'Brien, J. Clemmons, D. Baker, H. Spence, and G. Reeves (2015), Van Allen Probes show that the inner radiation zone contains no mev electrons: ECT/MagEIS data, *Geophys. Res. Lett.*, *42*(5), 1283–1289, doi:10.1002/2014GL062874.
Fok, M.-C., J. Kozyra, A. Nagy, C. Rasmussen, and G. Khazanov (1993), Decay of equatorial ring current ions and associated aeronomical consequences, *J. Geophys. Res.*, *98*(A11), 19,381–19,393, doi:10.1029/93JA01848.
Fok, M.-C., R. Horne, N. Meredith, and S. Glauert (2008), Radiation Belt Environment model: Application to space weather nowcasting, *J. Geophys. Res.*, *113*, A03S08, doi:10.1029/2007JA012558.
Ganushkina, N., T. Pulkkinen, A. Milillo, and M. Liemohn (2006), Evolution of the proton ring current energy distribution during 21–25 April 2001 storm, *J. Geophys. Res.*, *111*, A11S08, doi:10.1029/2006JA011609.
Ganushkina, N., M. Liemohn, and T. Pulkkinen (2012), Storm-time ring current: Model-dependent results, *Ann. Geophys.*, *30*, 177–202, doi:10.5194/angeo-30-177-2012.
Glauert, S., R. Horne, and N. Meredith (2014), Three-dimensional electron radiation belt simulations using the BAS radiation belt model with new diffusion models for chorus, plasmaspheric hiss, and lightning-generated whistlers, *J. Geophys. Res. Space Physics*, *119*, 268–289, doi:10.1002/2013JA019281.
Godunov, S. (1959), A difference method for numerical calculation of discontinuous solutions of the equations of hydrodynamics, *Matematicheskii Sbornik*, *89*(3), 271–306.
Godunov, S., and V. Ryabenkii (1987), *Difference Schemes: An Introduction to the Underlying Theory*, Elsevier, New York.
Haerendel, G. (1968), Diffusion theory of trapped particles and the observed proton distribution, in *Earth's Particles and Fields; proceedings of the NATO Advanced Study Institute held at Freising, Germany*, vol. 1, edited by B. M. McCormac, 171 pp., Reinhold Book Corporation, New York.
Hesse, M., and J. Birn (1993), Three-dimensional magnetotail equilibria by numerical relaxation techniques, *J. Geophys. Res.*, *98*(A3), 3973–3982, doi:10.1029/92JA02905.
Hudson, M., S. Elkington, J. Lyon, M. Wiltberger, and M. Lessard (2001), Radiation belt electron acceleration by ULF wave drift resonance: Simulation of 1997 and 1998 storms, in *Space Weather*, edited by P. Song, H. J. Singer, and G. L. Siscoe, AGU, Washington, D. C., doi:10.1029/GM125p0289.
Ilie, R., M. Liemohn, G. Toth, and R. Skough (2012), Kinetic model of the inner magnetosphere with arbitrary magnetic field, *J. Geophys. Res.*, *117*, A04208, doi:10.1029/2011JA017189.
Jordanova, V., L. Kistler, J. Kozyra, G. Khazanov, and A. Nagy (1996), Collisional losses of ring current ions, *J. Geophys. Res.*, *101*(A1), 111–126, doi:10.1029/95JA02000.
Jordanova, V., J. Kozyra, A. Nagy, and G. Khazanov (1997), Kinetic model of the ring current-atmosphere interactions, *J. Geophys. Res.*, *102*(A7), 14,279–14,291, doi:10.1029/96JA03699.
Kellogg, P. (1959), Van Allen radiation of solar origin, *Nature*, *183*, 1295–1297, doi:10.1038/1831295a0.
Kennel, C., and F. Engelmann (1966), Velocity space diffusion from weak plasma turbulence in a magnetic field, *Phys. Fluids*, *9*(12), 2377–2388, doi:10.1063/1.1761629.
Kersten, T., R. Horne, S. Glauert, N. Meredith, B. Fraser, and R. Grew (2014), Electron losses from the radiation belts caused by EMIC waves, *J. Geophys. Res. Space Physics*, *119*, 8820–8837, doi:10.1002/2014JA020366.
Kim, K.-C., Y. Shprits, D. Subbotin, and B. Ni (2011), Understanding the dynamic evolution of the relativistic electron slot region including radial and pitch angle diffusion, *J. Geophys. Res.*, *116*(A10), A10214, doi:10.1029/2011JA016684.
Lanzerotti, L., and C. Morgan (1973), ULF geomagnetic power near $l = 4$: 2. Temporal variation of the radial diffusion coefficient for relativistic electrons, *J. Geophys. Res.*, *78*(22), 4600–4610, doi:10.1029/JA078i022p04600.
Lemon, C., R. Wolf, T. Hill, S. Sazykin, R. Spiro, F. Toffoletto, J. Birn, and M. Hesse (2004), Magnetic storm ring current injection modeled with the Rice Convection model and a self-consistent magnetic field, *Geophys. Res. Lett.*, *31*, L21801, doi:10.1029/2004GL020914.
Leonard, B. (1991), The ULTIMATE conservative difference scheme applied to unsteady one-dimensional advection, *Comput. Meth. Appl. Mech. Eng.*, *88*(1), 17–74, doi:10.1016/0045-7825(91)90232-U.
Leonard, B., and H. Niknafs (1991), Sharp monotonic resolution of discontinuities without clipping of narrow extrema, *Comput. Fluids*, *19*(1), 141–154, doi:10.1016/0045-7930(91)90011-6.
Lerche, I. (1968), Quasilinear theory of resonant diffusion in a magnetoactive, relativistic plasma, *Phys. Fluids*, *11*, 1720–1727, doi:10.1063/1.1692186.
Li, X., D. Baker, M. Temerin, G. Reeves, and R. Belian (1998), Simulation of dispersionless injections and drift echoes of energetic electrons associated with substorms, *Geophys. Res. Lett.*, *25*(20), 3763–3766, doi:10.1029/1998GL900001.
Liemohn, M., J. Kozyra, C. Clauer, and A. Ridley (2001), Computational analysis of the near-earth magnetospheric current system during two-phase decay storms, *J. Geophys. Res.*, *106*(A12), 29,531–29,542, doi:10.1029/2001JA000045.
Liemohn, M., A. Ridley, D. Gallagher, D. Ober, and J. Kozyra (2004), Dependence of plasmaspheric morphology on the electric field description during the recovery phase of the 17 April 2002 magnetic storm, *J. Geophys. Res.*, *109*, A03209, doi:10.1029/2003JA010304.
Marchuk, G. (1990), Splitting and alternating direction methods, *Handb. Numer. Anal.*, *1*, 197–462.

Maynard, N., and A. Chen (1975), Isolated cold plasma regions: Observations and their relation to possible production mechanisms, *J. Geophys. Res.*, *80*(7), 1009–1013, doi:10.1029/JA080i007p01009.
Pfitzer, K., and J. Winckler (1968), Experimental observation of a large addition to electron inner radiation belt after a solar flare event, *J. Geophys. Res.*, *73*(17), 5792–5797, doi:10.1029/JA073i017p05792.
Press, W., S. Teukolsky, W. Vetterling, and B. Flannery (1992), *Numerical Recipes in C*, 2nd ed., Cambridge Univ. Press, New York.
Polyanin, A. (2001), *Handbook of Linear Partial Differential Equations for Engineers and Scientists*, Chapman and Hall/CRC Press, Boca Raton, Fla.
Roederer, J. (1970), *Dynamics of Geomagnetically Trapped Radiation*, Springer, New York.
Rothwell, P., and C. McIlwain (1960), Magnetic storms and the Van Allen radiation belts—Observations from satellite, *J. Geophys. Res.*, *65*, 799–806, doi:10.1029/JZ065i003p00799.
Russell, C., and R. Thorne (1970), On the structure of the inner magnetosphere, *Cosmic Electrodyn.*, *1*, 67–89.
Sarris, T., X. Li, N. Tsaggas, and N. Paschalidis (2002), Modeling energetic particle injections in dynamic pulse fields with varying propagation speeds, *J. Geophys. Res.*, *107*(A3), 1033, doi:10.1029/2001JA900166.
Schulz, M., and A. Eviatar (1969), Diffusion of equatorial particles in the outer radiation zone, *J. Geophys. Res.*, *74*, 2182–2192, doi:10.1029/JA074i009p02182.
Schulz, M., and L. Lanzerotti (1974), *Particle Diffusion in the Radiation Belts*, Springer, New York.
Shprits, Y., R. Thorne, G. Reeves, and R. Friedel (2005), Radial diffusion modeling with empirical lifetimes: Comparison with CRRES observations, in *Annales Geophysicae*, vol. 23, pp. 1467–1471, doi:10.5194/angeo-23-1467-2005.
Shprits, Y., R. Thorne, R. Friedel, G. Reeves, J. Fennell, D. Baker, and S. Kanekal (2006a), Outward radial diffusion driven by losses at magnetopause, *J. Geophys. Res.*, *111*, A11214, doi:10.1029/2006JA011657.
Shprits, Y., R. Thorne, R. Horne, S. Glauert, M. Cartwright, C. Russell, D. Baker, and S. Kanekal (2006b), Acceleration mechanism responsible for the formation of the new radiation belt during the 2003 Halloween solar storm, *Geophys. Res. Lett.*, *33*, L05104, doi:10.1029/2005GL024256.
Shprits, Y., D. Subbotin, N. Meredith, and S. Elkington (2008a), Review of modeling of losses and sources of relativistic electrons in the outer radiation belts: II. Local acceleration and loss, *J. Atmos. Sol. Terr. Phys.*, *70*(14), 1694–1713, doi:10.1016/j.jastp.2008.06.014.
Shprits, Y., N. Elkington, N. Meredith, and D. Subbotin (2008b), Review of modeling of losses and sources of relativistic electrons in the outer radiation belts: I. Radial transport, *J. Atmos. Sol. Terr. Phys.*, *70*(14), 1679–1693, doi:10.1016/j.jastp.2008.06.014.
Shprits, Y., D. Subbotin, and B. Ni (2009), Evolution of electron fluxes in the outer radiation belt computed with the VERB code, *J. Geophys. Res.*, *114*, A11209, doi:10.1029/2008JA013784.
Shprits, Y., D. Subbotin, B. Ni, R. Horne, D. Baker, and P. Cruce (2011), Profound change of the near-Earth radiation environment caused by solar superstorms, *Space Weather*, *9*, S08007, doi:10.1029/2011SW000662.
Shprits, Y., D. Subbotin, A. Drozdov, M. Usanova, A. Kellerman, K. Orlova, D. Baker, D. Turner, and K.-C. Kim (2013), Unusual stable trapping of the ultrarelativistic electrons in the Van Allen radiation belts, *Nat. Phys.*, *9*(11), 699–703, doi:10.1038/nphys2760.
Shprits, Y., A. Kellerman, A. Drozdov, H. Spence, G. Reeves, and D. Baker (2015), Combined convective and diffusive simulations: VERB-4D comparison with 17 March 2013 Van Allen Probes observations, *Geophys. Res. Lett.*, *42*(22), 9600–9608, doi:10.1002/2015GL065230.
Shue, J.-H., J. Chao, H. Fu, C. Russell, P. Song, K. Khurana, and H. Singer (1997), A new functional form to study the solar wind control of the magnetopause size and shape, *J. Geophys. Res.*, *102*(A5), 9497–9511, doi:10.1029/97JA00196.
Stern, D. (1975), The motion of a proton in the equatorial magnetosphere, *J. Geophys. Res.*, *80*(4), 595–599, doi:10.1029/JA080i004p00595.
Strang, G. (2007), *Computational Science and Engineering*, vol. 1, Wellesley-Cambridge Press, Wellesley.
Subbotin, D., and Y. Shprits (2009), Three-dimensional modeling of the radiation belts using the Versatile Electron Radiation Belt (VERB) code, *Space Weather*, *7*, S10001, doi:10.1029/2008SW000452.
Subbotin, D., and Y. Shprits (2012), Three-dimensional radiation belt simulations in terms of adiabatic invariants using a single numerical grid, *J. Geophys. Res.*, *117*, A05205, doi:10.1029/2011JA017467.
Subbotin, D., Y. Shprits, and B. Ni (2010), Three-dimensional VERB radiation belt simulations including mixed diffusion, *J. Geophys. Res.*, *115*, A03205, doi:10.1029/2009JA015070.
Subbotin, D., Y. Shprits, M. Gkioulidou, L. Lyons, B. Ni, V. Merkin, F. Toffoletto, R. Thorne, R. Horne, and M. Hudson (2011a), Simulation of the acceleration of relativistic electrons in the inner magnetosphere using RCM-VERB coupled codes, *J. Geophys. Res.*, *116*, A08211, doi:10.1029/2010JA016350.
Subbotin, D., Y. Shprits, and B. Ni (2011b), Long-term radiation belt simulation with the VERB 3-D code: Comparison with CRRES observations, *J. Geophys. Res.*, *116*, A08211, doi:10.1029/2011JA017019.
Sweby, P. (1984), High resolution schemes using flux limiters for hyperbolic conservation laws, *SIAM J. Numer. Anal.*, *21*(5), 995–1011, doi:10.1137/0721062.
Thorne, R., and C. Kennel (1971), Relativistic electron precipitation during magnetic storm main phase, *J. Geophys. Res.*, *76*(19), 4446–4453, doi:10.1029/JA076i019p04446.
Toffoletto, F., S. Sazykin, R. Spiro, and R. Wolf (2003), Inner magnetospheric modeling with the Rice Convection model, *Adv. Space Environ. Res.*, *107*(1), 175–196, doi:10.1023/A:1025532008047.
Tsyganenko, N., and T. Mukai (2003), Tail plasma sheet models derived from Geotail particle data, *J. Geophys. Res.*, *108*(A3), 1136, doi:10.1029/2002JA009707.
Tu, W., G. Cunningham, Y. Chen, M. Henderson, E. Camporeale, and G. Reeves (2013), Modeling radiation belt electron dynamics during GEM challenge intervals with the DREAM3D diffusion model, *J. Geophys. Res. Space Physics*, *118*(10), 6197–6211, doi:10.1002/jgra.50560.
Usanova, M., et al. (2014), Effect of EMIC waves on relativistic and ultrarelativistic electron populations: Ground-based and Van Allen probes observations, *Geophys. Res. Lett.*, *41*(5), 1375–1381, doi:10.1002/2013GL059024.
Vernov, S., et al. (1969), Particle fluxes in outer geomagnetic field, *Rev. Geophys.*, *7*(1–2), 257–280, doi:10.1029/RG007i001p00257.
Volland, H. (1973), A semiempirical model of large-scale magnetospheric electric fields, *J. Geophys. Res.*, *78*(1), 171–180, doi:10.1029/JA078i001p00171.
Walt, M. (1994), *Introduction to Geomagnetically Trapped Radiation*, Cambridge Univ. Press, New York.
Williams, D., and A. Smith (1965), Daytime trapped electron intensities at high latitudes at 1100 kilometers, *J. Geophys. Res.*, *70*, 541–556, doi:10.1029/JZ070i003p00541.
Zalesak, S. (1987), *Advances in Computer Methods for Partial Differential Equations VI*, IMACS, Rutgers Univ., New Brundswick, N. J.
Zhang, Y., H. Zhu, L. Zhang, Y. He, Z. Gao, Q. Zhou, C. Yang, and F. Xiao (2014), Effect of low energy electron injection on storm-time evolution of radiation belt energetic electrons: Three-dimensional modeling, *Astrophys. Space Sci.*, *352*(2), 613–620, doi:10.1007/s10509-014-1984-x.